Supplemental Information for

Observations of thermodynamics and hydrodynamics in an atoll system and their influence on coral cover

Justin S. Rogers, Stephen G. Monismith, David A. Koweek, Walter I. Torres, and Robert B. Dunbar

Limnology and Oceanography

1. Instrumentation

Details of field deployment dates, locations and instrumentations are in Table SI 1. The primary field results used for this analysis are from September 2012 to July 2014, with results from September 2011 to September 2012 not used in this analysis due to lower spatial and temporal resolution.

2. Tides and Circulation

On the exterior of the atoll, the tidal amplitude of the free surface of the M2 tide was 0.30 m. With propagation into the lagoon system (East Lagoon), the amplitude decreased to 0.26 m, and the phase lagged by up to 4.7 hours (Figure SI 1a). The results were similar for the K1 tide, with 0.08 m amplitude on the reef exterior, decreased to 0.07 m with 6.0 hr phase lag in the East Lagoon. The current ellipses show flow was generally aligned with bathymetric contours, except on the terrace. The contribution of the M2 tide to flow was relatively small on the forereef (< 20% of overall velocity), while on the western terrace and channel the contribution was large (> 50% of overall velocity) (Figure SI 1b). The net mean flow over the measurement period was to the west on the south forereef, out of the lagoon in the channel, near zero on the western terrace, and to the east on the north forereef (Figure SI 1b). See Section 3.3 for discussion of wave driven flow through the lagoon system and note that net gage spatial coverage is not complete enough to conserve mass. In summary, tidal forcing was most important at the field sites near the atoll interior, and the oscillations generally follow the alongshore bathymetric contours. The free surface tidal amplitude was only slightly reduced with propagation into the lagoon system, but

was significantly delayed by up to 4.3 hours in the interior East Lagoon due to the constricted inlets (Figure S1 1a).

3. Bottom roughness and drag estimation

Flow within coral systems is complex because they have irregular, branching morphologies with reef topography varying at scales ranging from centimeters to kilometers (Rosman and Hench 2011). In circulation models, variability in reef geometry occurs at scales smaller than the resolution of the computational grid; thus, drag due to the small-scale geometry must be parameterized. A typical method of parameterization is a log-layer roughness height including the effects of waves (Madsen 1994). On reefs, bottom friction is often a significant term in the momentum balance and the primary dissipation loss; and thus correct parameterization of the bottom drag is essential (Monismith 2007).

We employed an empirical orthogonal function (EOF) analysis on the measured velocity profiles at each site to decompose the signal into its principal components, or dominant statistical modes. The EOF analysis provides a description of the spatial variability of the velocity field through the modal shapes (eigenfunctions), as well as the temporal variability through the modal amplitude time series (Emery and Thomson 2004). The first mode of the empirical orthogonal functions (EOFs) of the velocity profiles in the alongshore directions explained (97, 97, 97, 98, 93, and 41%) of the variance and in the cross-shore directions explained (71, 56, 84, 83, 90, and 96%) of the variance for sites FR3, FR5, FR7, FR9, RT4, and CHAN respectively (Figure SI 2). At most of the sites, the deeper part of the profile was roughly linear, (note log scale), indicating a log-layer like flow (Figure S1 2). Near the surface on the forereef and channel sites, the profile deviated from the linear profile.

For a well-developed turbulent boundary layer, an inertial sublayer region exists where mean velocities exhibit a logarithmic profile. Within this region, the mean velocity profile is related to the generation of turbulence by shear at the bed, and the law of the wall takes the form (e.g., Reidenbach et al. 2006; Kundu and Cohen 2008):

$$\boldsymbol{u_E}(z,t) = \frac{\boldsymbol{u_*}(t)}{\kappa} \ln\left(\frac{z-\boldsymbol{d}}{\boldsymbol{z_{0a}}}\right) \qquad (SI\ 1)$$

Where $\boldsymbol{u}_*$ is the friction velocity, κ is von Karman's constant (0.41), $\boldsymbol{d}$ is the displacement height (MAB), and $\boldsymbol{z_{0a}}$ is the apparent bottom roughness length scale. In very rough boundary layers, it is not clear where $z = 0$ should be defined, and thus d is typically included in the fitting function (Rosman and Hench 2011). Values of u^*, d, and z_{0a} were adjusted to obtain a best fit using the least squares fit from measurement points from the ADP/ADCP measurements between the bottom and ½ of the depth. To ensure a well-defined log region over the measurement points used in the fit, only alongshore profiles having strong mean flow ($u_E > 5$cm/s), physically realistic roughness $0.001 < 30z_{0a} < 0.5h$, offset $0.01 < d < 1.25$ m, and good fit ($r^2 > 0.8$) were used in the analysis.

When waves are present, their high bottom shear stresses interact with the mean flow boundary layer which acts to increase the bottom roughness felt by the mean current, therefore the apparent roughness scale (z_{0a}) is larger than the physical roughness scale (z_0) (Grant and Madsen 1979). Using this theory with the wave and near bed velocity data, z_{0a} and computed reference height ($z_{ref} - d$) from the log fit, the physical roughness $k_N = 30z_0$ was iterated until z_{0a} from both methods matched within 1%. Only physically realistic values of k_N were kept, $0.01 < k_N < 2$ m. The mean z_{0a}, d, and k_N were computed as the log-mean of the results from each deployment period, i.e. $z_{0a} = exp\left(\overline{\ln z_{0a}(t)}\right)$ (Reidenbach et al. 2006).

Using a log-layer fit to the measured velocity profiles (Eq. SI 1) the two-day low pass filtered $\overline{z_{0a}}$ at the north forereef (FR9) increases with increased wave height, as expected (Figure SIa). The results for d, z_{oa}, and z_o are highly variable, and their distributions are typically exponential thus confirming the use of the log mean for statistics. An example of these distributions at the FR9 site is shown in Figure SI 3b,c,d. Over all the sites, offset height d varied from 24 to 86 cm, the apparent z_{0a} varied from 1.2 cm to 5.5 cm, and the physical roughness height z_0, (removing the effects of waves where applicable), varied from 0.17 to 3.7 cm (Table SI 2).

For several short-term experiments (NFR13, CHAN, Figure SI) using ADVs with a high sampling rate, mean bottom stress, $\boldsymbol{\tau_b}$, was computed from the turbulent Reynolds stress, which are assumed constant within the inertial sublayer, (e.g. Reidenbach et al. 2006),

$$\boldsymbol{\tau_b} = -\rho\overline{\boldsymbol{u}'w'} \qquad (SI\ 2)$$

using the measured turbulent velocities ($\boldsymbol{u'}$) from the ADVs. A common bottom stress parameterization is given by (e.g., Grant and Madsen 1979; Feddersen et al. 2000),

$$\boldsymbol{\tau_b} = \rho \boldsymbol{C_D} \overline{\boldsymbol{u}|\boldsymbol{u}|} \qquad (SI\ 3)$$

where $\boldsymbol{u}$ is evaluated near the bed but above the bottom boundary layer, and $\boldsymbol{C_D}$ is a nondimensional drag coefficient which may depend on the flow environment, height above the bed and bottom roughness. Combining Eqns. (SI 2) and (SI 3) gives,

$$\boldsymbol{C_D} = \frac{-\overline{\boldsymbol{u'}w'}}{\overline{\boldsymbol{u}|\boldsymbol{u}|}} \qquad (SI\ 4)$$

where in environments with low wave and turbulence energy, the denominator is often simplified to $\overline{\boldsymbol{u}}|\overline{\boldsymbol{u}}|$, and $\overline{\boldsymbol{u}}$ is either the depth averaged or near bed velocity, see Rosman and Hench (2011) for a complete discussion. Results using this method for bottom drag coefficient C_D using Reynolds stress (Eq. SI 4) varied from 0.0037 (CHAN) to 0.10 (NFR13) (Table SI 2).

List of References

Emery, W. J., and R. E. Thomson. 2004. Data analysis methods in physical oceanography, 2nd ed. Elsevier.

Feddersen, F., R. T. Guza, S. Elgar, and T. H. C. Herbers. 2000. Velocity moments in alongshore bottom stress parameterizations. J. Geophys. Res. **105**: 8673. doi:10.1029/2000JC900022

Grant, W. D., and O. S. Madsen. 1979. Combined wave and current interaction with a rough bottom. J. Geophys. Res. **84**: 1797. doi:10.1029/JC084iC04p01797

Kundu, P. K., and I. M. Cohen. 2008. Fluid Mechanics, 4th ed. Academic Press.

Madsen, O. S. 1994. Spectral Wave-Current Bottom Boundary Layer Flows. Coast. Eng. Proc. **1**: 384–398. doi:10.9753/icce.v24.

Monismith, S. G. 2007. Hydrodynamics of Coral Reefs. Annu. Rev. Fluid Mech. **39**: 37–55. doi:10.1146/annurev.fluid.38.050304.092125

Reidenbach, M. a., S. G. Monismith, J. R. Koseff, G. Yahel, and A. Genin. 2006. Boundary layer turbulence and flow structure over a fringing coral reef. Limnol. Oceanogr. **51**: 1956–1968. doi:10.4319/lo.2006.51.5.1956

Rogers, J. S., S. G. Monismith, R. B. Dunbar, and D. Koweek. 2015. Field observations of wave-driven circulation over spur and groove formations on a coral reef. J. Geophys. Res. Ocean. **120**: 145–160. doi:10.1002/2014JC010464

Rosman, J. H., and J. L. Hench. 2011. A framework for understanding drag parameterizations for coral reefs. J. Geophys. Res. Ocean. **116**: 1–15. doi:10.1029/2010JC006892

Figures and Tables

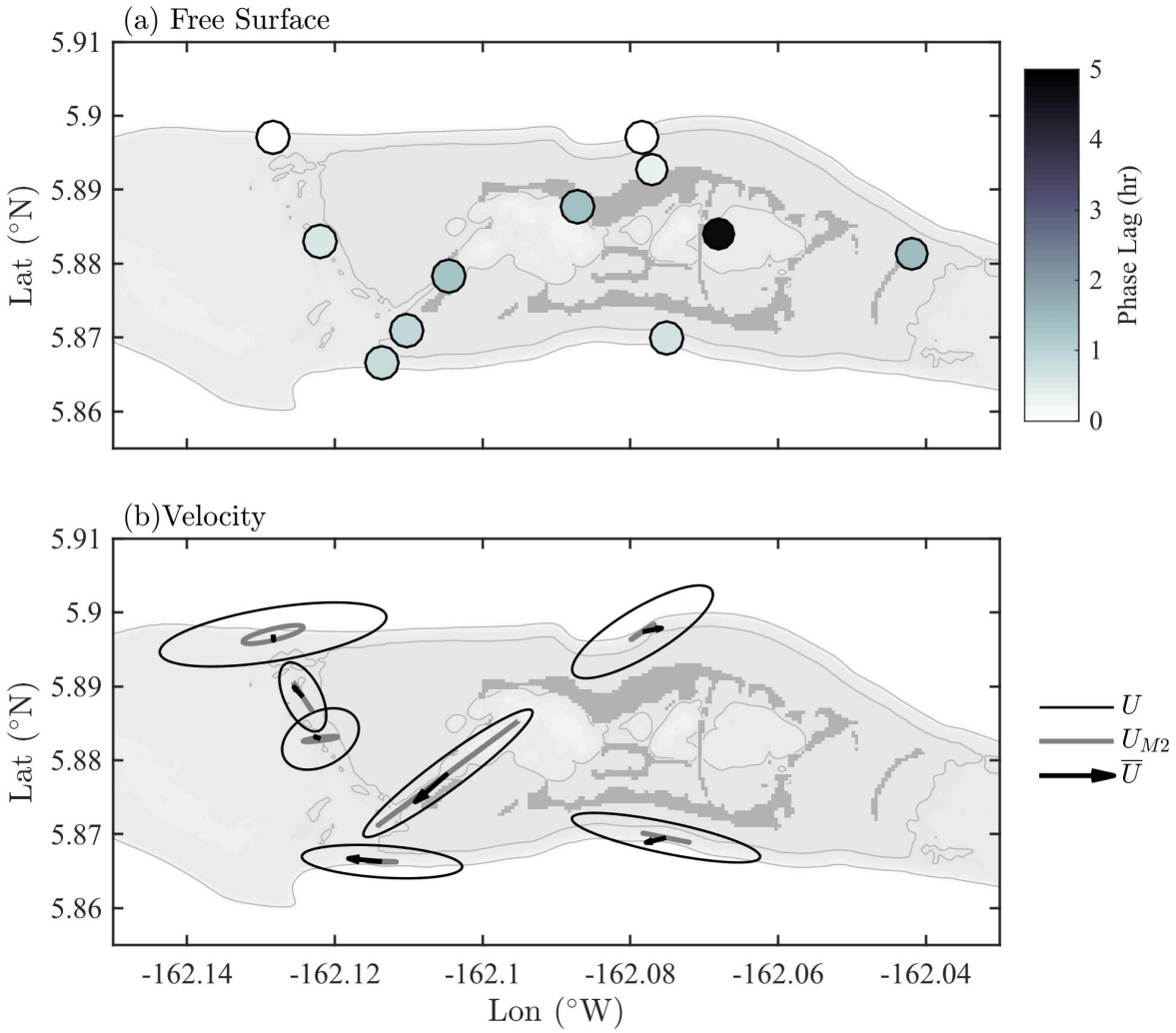

Figure SI 1. Measured tidal amplitude, flow averages and current ellipses. Amplitude (size) and phase lag (color) of M2 tide from surface ζ, (b) depth averaged Lagrangian velocity U ellipses, M2 tidal velocity U_{M2} ellipse, average flow $\overline{U}$ vector over the measurement record. Light gray lines are 5 and 60 m depth contours, light gray shading is land mask. Velocity ellipses are one standard deviation of velocity.

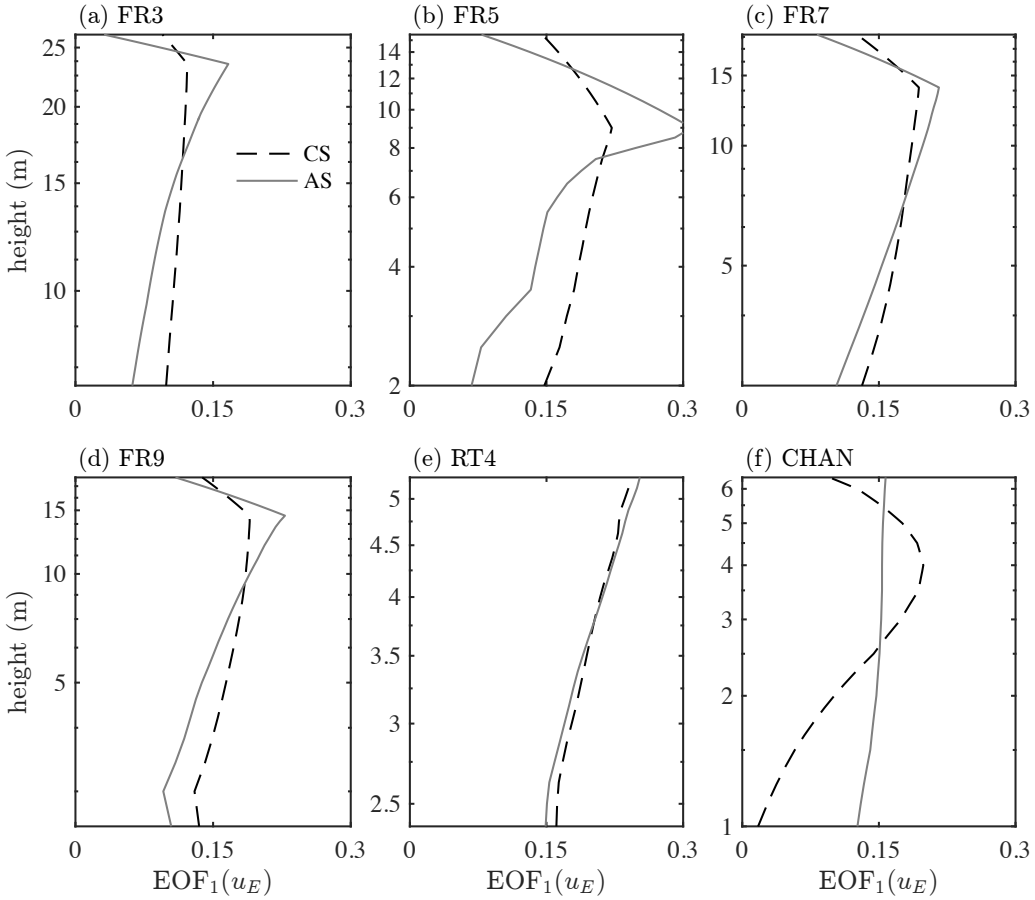

Figure SI 2. First empirical orthogonal function (EOF_1) of measured Eulerian velocity profiles u_E with height above bottom at six sites, (a) FR3, (b) FR5, (c) FR7, (d) FR9, (e) RT4, and (f) CHAN, in cross-shore (CS) and alongshore (AS) directions. Note log scale with depth.

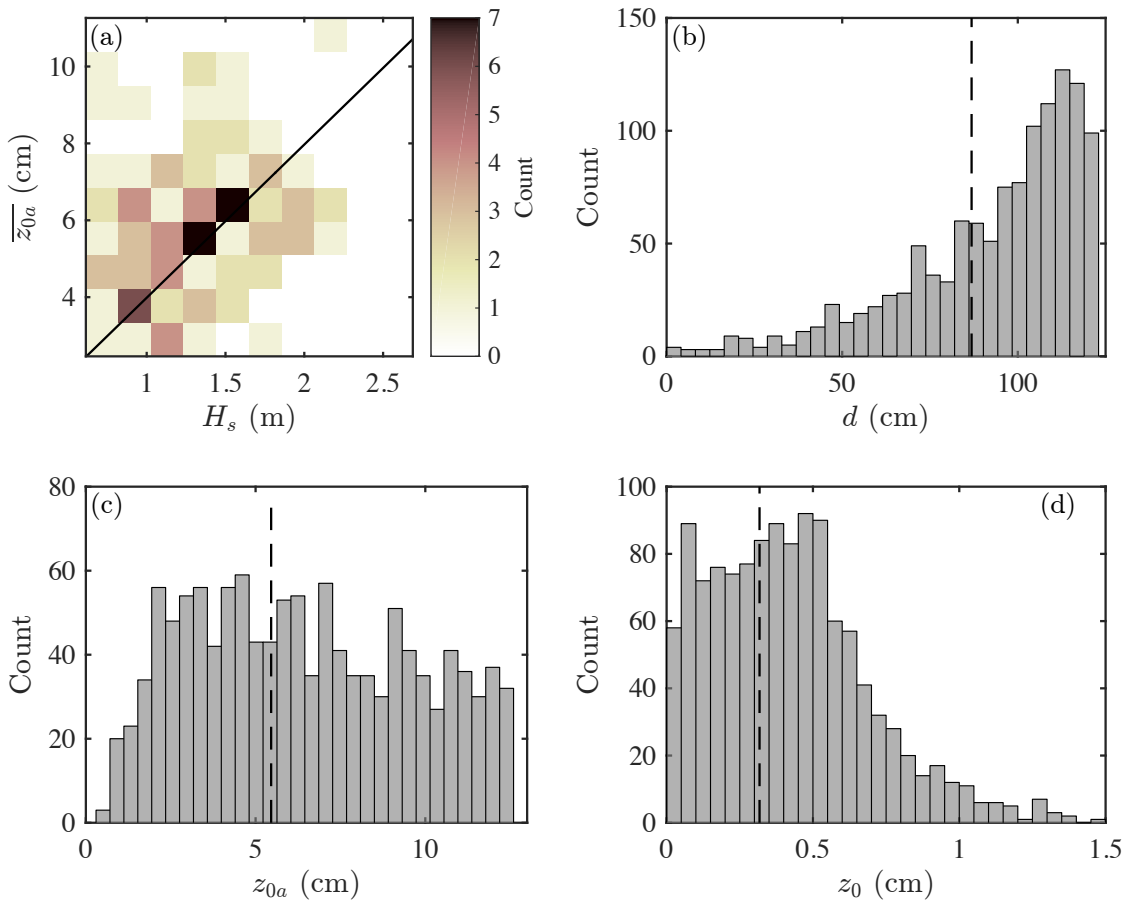

Figure SI 3. Bottom roughness results on north forereef (FR9) as a function of wave height. Computed apparent bottom roughness $\overline{z_{0a}}$ (two day filtered) and significant wave height H_s Sep-2013 to May-2014, and distributions (b) offset height d, (c) apparent roughness height z_{0a}, and (d) roughness height z_0. Black solid line in (a) is a best fit to data, black dashed line in (b-d) is the log-mean of each variable.

Table SI 1. Field experiment instrumentation, depth, deployment time, and sampling at each site.

	Site	*h* (m)	Dates[1]	Instrument (sampling rate)[2,3]
Forereef	FR3	30.5	Oct-11 – Oct-12	RDI ADCP (15 min), RBR 1050 (10 s)
			Oct-12 – Sep-13	RDI ADCP (5 min), RBR Virtuoso (2 s), 3-SBE 56, SBE 37 (2 min)
			Sep-13 – Jul-14	RBR Virtuoso (2 s), 3-SBE 56, SBE 37 (12 min)
			16-23 Jul-14	Nortek ADP (2 s), RBR 1050 (2 s)
	FR5	20.1	Oct-12 – Sep-13	Nortek ADP (5 min, & burst: 1 s for 1024 s), RBR Virtuoso (2 s), 3-SBE 56
			Sep-13 – Jul-14	Nortek ADP (5 min, & burst: 1 s for 1024 s), 3-SBE 56
	FR7	22.5	Oct-11 – Oct-12	RBR 1050, (10 s), SBE 37 (2 min)
			Oct-12 – Sep-13	RDI ADCP (5 min), 3-SBE 56, SBE 37 (2 min)
			Sep-13 – Jul-14	RDI ADCP (2 min), 3-SBE 56
	FR9	11.5	Oct-12 – Sep-13	RDI ADCP (5 min), RBR Virtuoso (2 s), 3-SBE 56
			Sep-13 – Jul-14	RDI ADCP (2 min), RBR Virtuoso (2 s), 3-SBE 56
Western Terrace	PSM	5.9	Oct-12 – Sep-13	RBR 1050 (12 s), SBE 56
			Sep-13 – Jul-14	RBR 1050 (14 s), SBE 56
	RT4	4.9	Oct-11 – Oct-12	RDI ADCP (15 min)
			Oct-12 – Sep-13	Nortek ADV (10 min), SBE 56, SBE 37 (2 min)
			Sep-13 – Jul-14	Nortek ADV (10 min), RBR Virtuoso, (2 s), SBE 56
	RT10	3.0	Oct-12 – Sep-13	Nortek ADV (10 min), SBE 56
			Sep-13 – Jul-14	Nortek ADV (10 min), RBR Virtuoso, (2 s), SBE 56
	RT13	3.7	Oct-12 – Sep-13	RBR 1050 (12 s), SBE 56
			Sep-13 – Jul-14	SBE 56
Reef Flat	NB	3.9	Oct-11 – Oct-12	RBR 1050, (10 s), SBE 56
			Oct-12 – Sep-13	RBR 1050, (12 s) , SBE 56
			Sep-13 – Jul-14	RBR 1050, (14 s) , SBE 56
	NBE	0.55	Sep-13 – Jul-14	RBR 1050, (14 s) , SBE 56
Lagoons	BE	2.4	Oct-12 – Sep-13	RBR 1050, (12 s) , SBE 56
			Sep-13 – Jul-14	SBE 56
	CHAN	7.7	Oct-11 – Oct-12	RDI ADCP (15 min), 4-SBE 56
			Oct-12 – Sep-13	Nortek ADP (5 min, & burst: 1 s for 1024 s), 3-SBE 56
			Sep-13 – Jul-14	Nortek ADP (15 min), 3-SBE 56, SBE 37 (12 min)
			19-24 Jul-14	Nortek ADV (0.125 s)
	DOCK	3.5	Oct-11 – Oct-12	RBR 1050 (14 s)
			Oct-12 – Sep-13	SBE 56
			Sep-13 – Jul-14	RBR 1050 (14 s), SBE 56

EL	1.9	Oct-12 – Sep-13	RBR 1050, (14 s), SBE 56
		Sep-13 – Jul-14	RBR 1050, (14 s), SBE 56

1. Deployment and recovery were in Oct 2011, Oct 2012, Sept 2013, and July 2014 with typically two week maintenance downtime.
2. All SBE 56 instruments sampled at 10 s.
3. Additional sites with only SBE 56 thermistors,
    a. Oct-11 – Oct-12: RT1(5),
    b. Oct-12 – Sep-13: CG, CC, LL, OCM, PSI, PSO, RT1, SIB, TG, WCG, WL(5);
    c. Sep-13 – Jul-14: CG, CC, OCM(3),PSI, PSO, RT1, RP, TG, WL(5)

Table SI 2. Bottom roughness and drag results from field measurements at various sites using fits to velocity profiles, and Reynolds stress.

				Log Layer Fit						Reynolds Stress	
	Site	**Waves?**	***h* (m)**	***d* (cm)**		***z₀* app (cm)**		***z₀* (cm)[1]**		***C_D***	
Forereef	FR3	Yes	29	40	±21	3.4	±3.6	0.33	±0.32		
	FR5	Yes	20	66	±18	3.5	±1.9	0.26	±0.10		
	FR7	Yes	22	62	±25	4.3	±2.0	0.24	±0.10		
	FR9	Yes	21	86	±19	5.5	±1.9	0.32	±0.13		
	NFR13 C1	Yes	19	17	±28	2.2	±1.6	0.40	±0.33		
Spur and Groove	NFR13 Spur	Yes	9	40	±16	2.3	±1.1	0.17	±0.14	0.0072	±0.0007
	NFR13 Groove	Yes	11	63	±7	5.0	±1.9	0.19	±0.08	0.10	±0.007
	SFR12 Spur	Yes	9	24	±19	3.3	±1.4	0.17	±0.16		
	SFR12 Groove	Yes	11	34	±23	2.9	±1.1	0.18	±0.13		
Terrace	SIB	No	4	35	±12	3.7	±1.0	3.7	±1.0		
Lagoon	CHAN	No	8	24	±9	1.2	±0.8	1.2	±0.8	0.0037	±0.0004

1. Using Grant and Madsen (1979) to remove wave effects, $z_0 = k_N/30$.
2. Results are averaged over best available data at each site, and uncertainties are reported as one standard deviation.
3. For NFR13 study details, see (Rogers et al. 2015).